Experimental and Numerical Study on the Bead-Carry-Out in Two Component Development Process in Electrophotography

Nobuyuki Nakayama, Yoichi Watanabe and Yasuaki Watanabe
Research and Development Center, Fuji Xerox Co., Ltd., Nakai-machi, Kanagawa, JAPAN

Hiroyuki Kawamoto✦
Department of Mechanical Engineering, Waseda University, Shinjuku, Tokyo, JAPAN

Experimental and numerical investigations have been carried out on the bead-carry-out phenomenon of electromagnetic bead chains in two component development process of electrophotography. Electrostatic pull-off characteristics of chains were measured in a magnetic field and then it was clarified how the critical electrostatic pull-off field to break chains and the amount of pulled-off carriers depended on the bead diameter and the magnetic field. Magnetic bonding force and electrostatic pull-off force were estimated numerically to evaluate these experimental results. It was deduced that the bead-carry-out phenomenon could be predicted qualitatively from the comparison of calculated magnetic and electrostatic force.

Journal of Imaging Science and Technology 49: 539–544 (2005)

Introduction

Although there are several types of the development subsystem in electrophotography, such as magnetic single component development, two component magnetic brush development, and nonmagnetic single component development, the two component development process is most widely used in high speed and/or color laser printers because it can realize high image quality and high reliability.[1] A schematic drawing of this system is shown in Fig. 1. Magnetized carrier beads form chain clusters on a rotatory sleeve in the magnetic field created by a stationary permanent magnet. Toner particles electrostatically attached to magnetic bead chains are transported to the development zone with rotation of the sleeve. In the development zone, electrostatic force acts on toner particles and they move to electrostatic latent images on photoreceptor surface to form real images.

The electrostatic force acts not only on toner particles but also on carrier chains and therefore carrier bead(s) are sometimes separated from chains and moved to photoreceptor surface. The phenomenon is well known as a bead-carry-out (BCO). Because the attached carrier beads on the photoreceptor surface cause significant image degradations, it is important to clarify the mechanism and requirements to prevent BCO. Williams first introduced this phenomenon and gave basic information in his textbook.[1] However, no literature has been published on this subject after the Williams' textbook, although it has been a well accepted consensus in an electrophotography community that the BCO is one of the most serious issues of the two component magnetic brush development system.

In this study, experimental and numerical investigations have been carried out on the BCO phenomenon to clarify the mechanism and effects of parameters such as the bead diameter and the magnetic field strength. In the experiment, a critical electrostatic pull-off field

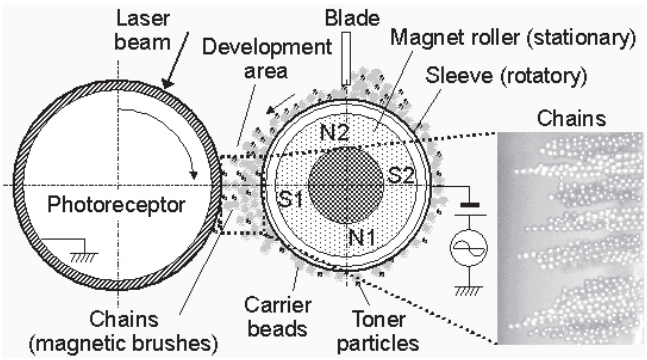

Figure 1. Two component development process for laser printers.

Original manuscript received January 29, 2004

✦IS&T Fellow

Corresponding author: N. Nakayama, Nobuyuki.Nakayama@fujixerox.co.jp

This article has been presented at The 19th International Congress on Digital Printing Technologies (NIP19) at New Orleans, Louisiana; September 29, 2003.

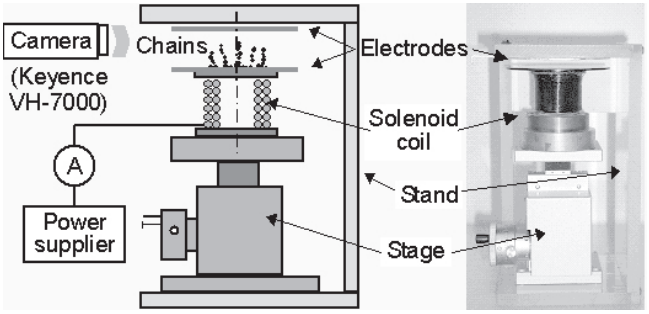

Figure 2. Experimental setup with solenoid coil.

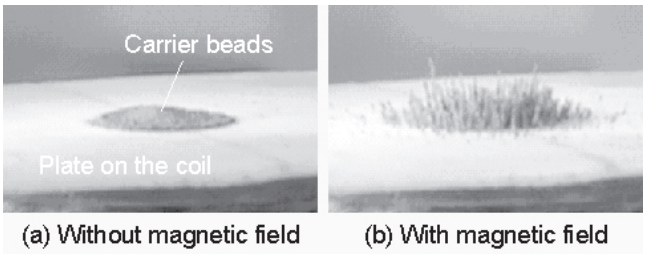

Figure 3. Photographs of magnetic carrier beads with and without magnetic field created by a coil.

to separate bead(s) from chains was measured and effects of the bead diameter and the magnetic field were evaluated. A solenoid coil was used in this experiment instead of the magnetic roller to create the controllable magnetic field. Amount of pulled-off carriers was also measured in another experiment with a magnet roller used in a commercially available color printer. In addition, two kinds of numerical simulation were performed to calculate magnetic bonding force between beads and electrostatic pull-off force based on the assumption that the BCO takes place when the electrostatic force exceeds the magnetic force. The numerical simulation of chain formation was performed to estimate magnetic bonding force between beads in the chain by the Distinct Element Method (DEM). On the other hand, an electrostatic pull-off force was estimated in the electric field with electroresistive chains by the Finite Element Method (FEM). These numerical results were compared to experimental results to evaluate adequacy of the assumption and to study pull-off characteristics.

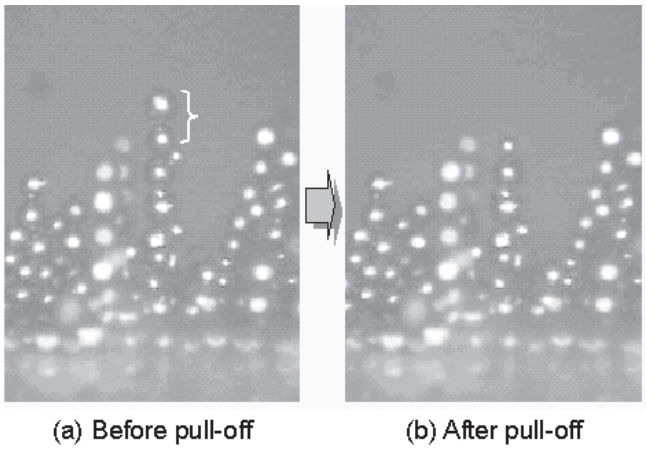

Figure 4. Photographs of chains before and after pull-off.

Experimental Method

Solenoid Coil System

Figure 2 shows an illustration and a photograph of an experimental setup with a solenoid coil to investigate the electrostatic pull-off phenomenon of chains.[2,3] Axial magnetic flux density B' along the center axis of the coil was measured and approximated by $B'(z) = B_0 (1 - cz)$, where B_0 and c (= 66.9 1/m) are constants and z is the axial coordinate. (z = 0 at the surface of the end plate on which carrier beads were mounted.) B_0 is proportional to the coil current with a proportional constant 6.16 mT/A. Spherical, soft magnetic, and conductive carriers were mounted at the center of the end plate on the solenoid coil in a 10 mm diameter area with 0.637 kg/m^2 in surface loading. These carriers were 35–107 μm in diameter, 3500–3620 kg/m^3 in volume density, and 4.2–4.7 in relative magnetic permeability. The electric field was applied quasi-statically to chains between a set of parallel electrodes with 6.0 mm in gap. If the sufficient electric field was applied, carrier beads at the top of chains were charged and pulled off by the electrostatic force. This transient motion of chains was observed by a digital microscope (Keyence Corp., VH-7000) and the critical voltage between electrodes to break chain was recorded. Photographs of chains before and after pull-off are shown in Fig. 4.

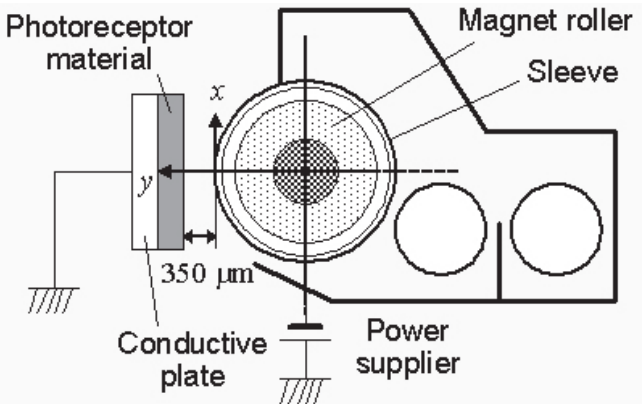

Figure 5. Experimental setup with magnet roller.

Magnet Roller System

Figure 5 shows another experimental setup with the magnet roller. In this experiment, non-spherical, soft magnetic, and conductive carriers without toner particles were provided on a development sleeve with 17.9 mm in diameter. A roller made of multi-pole permanent magnet was settled inside the development sleeve to form static magnetic field. The magnetic flux density distribution near the gap between the plate and the sleeve can be approximated by

$$B'(x, y) = (\alpha_1 x^2 + \alpha_2 x + \alpha_3 x)/(\beta_1 y^2 + \beta_2 y + \beta_3)$$

TABLE I. Coefficients of Magnetic Flux Density

Coefficient	B'_x	B'_y
α_1	0.0	-1.47×10^5
α_2	6.56×10^2	6.23
α_3	-2.09×10^{-1}	2.48
β_1	1.00×10^6	9.97×10^5
β_2	1.13×10^4	1.20×10^4
β_3	1.76×10^1	1.96×10^1

in the Cartesian coordinate system (x, y). The coefficients $\alpha_{1,2,3}$ and $\beta_{1,2,3}$ were determined by regression of measured distribution of the flux density as listed in Table I. Carriers used in this experiment were 35–80 μm in diameter, 5000 kg/m^3 in volume density, and 11.5 in relative magnetic permeability. The surface loading was 0.4 kg/m^2 on the sleeve in the vicinity of the development zone. A grounded conductive flat plate with a photoreceptor layer of 25 μm thickness was set close to the sleeve with 350 μm in gap. After the application of DC bias voltage to the sleeve, the plate was moved away from the sleeve to measure the amount of carrier beads attached on the photoreceptor surface.

Numerical Method

Magnetic bonding force and electrostatic pull-off force are the dominant forces applied to the magnetic and conductive carriers in development area as illustrated in Fig. 6. If the electrostatic force exceeds the magnetic force, the top of the chain will be separated. In this study, these two kinds of forces are numerically calculated by the following separated methods to evaluate the force balance that causes the BCO.

Magnetic Force

The DEM[2,4] was employed to simulate chain forming process and to estimate the magnetic bonding force. In the calculation, the following two-dimensional momentum equation is solved for each carrier bead.

$$m_j \ddot{\mathbf{u}}_j = \mathbf{F}_j \left(\mathbf{F}_j = \mathbf{F}_{cj} + \mathbf{F}_{mj} + 3\pi\eta a_j \dot{\mathbf{u}}_j + m_j \mathbf{g} \right), \qquad (1)$$

where m_j, $\mathbf{u}_j$, and $\mathbf{F}_j$ are mass, displacement vector (x_i, y_i), and applied force vector to the j-th bead, respectively. Mechanical contact force $\mathbf{F}_{cj}$, magnetic force $\mathbf{F}_{mj}$, air drag $3\pi\eta a_j \boldsymbol{u}_j$, and gravitational force $m_j \mathbf{g}$ are included in the applied force. Here, η is viscous coefficient of air, a_j is the diameter of the bead, and $\mathbf{g}$ designates the gravitational constant. Van der Waals force was neglected, because it is not dominant for particles more than ten microns in diameter.

The mechanical contact force was determined by the Foigt model. That is, the force in the normal direction at the contact point was estimated from the Hertzian theory and that in the tangential direction was assumed to be proportional to the normal force with a proportionality constant 0.25.

The magnetic force $\mathbf{F}_{mj}$ to the j-th bead with the magnetic dipole moment $\mathbf{p}_j$ are given by the following expression under the assumption that each bead behaves as a magnetic dipole placed at the center of the bead.[5]

$$\mathbf{F}_{mj} = \left(\mathbf{p}_j \cdot \nabla \right) \mathbf{B}_j \qquad (2)$$

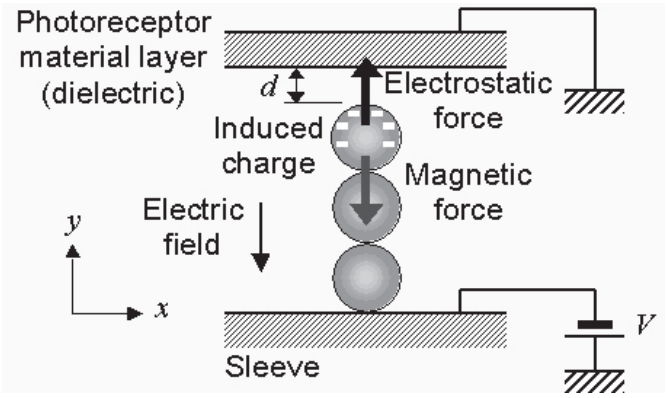

Figure 6. Applied forces to carrier beads in development area.

The magnetic flux density $\mathbf{B}_j$ at the position of the j-th bead and magnetic moment $\mathbf{p}_j$ are

$$\mathbf{B}_j = \mathbf{B}_j{}' + \sum_{\substack{k=1 \\ j \neq k}}^{N} \frac{\mu_0}{4\pi} \left(\frac{3\left(\mathbf{p}_k \cdot \mathbf{r}_{kj}\right)}{\left|\mathbf{r}_{kj}\right|^5} \mathbf{r}_{kj} - \frac{\mathbf{p}_k}{\left|\mathbf{r}_{kj}\right|^3} \right), \qquad (3)$$

$$\mathbf{p}_j = \frac{4\pi}{\mu_0} \frac{\mu - 1}{\mu + 2} \frac{{a_j}^3}{8} \mathbf{B}_j, \qquad (4)$$

where N is the number of particles, μ_0 is the permeability of free space, μ is the relative permeability of beads, and $\boldsymbol{r}_{kj}$ is the position vector from the k-th to the j-th bead.

Electrostatic Force

The electrostatic force to break the chain can be estimated by the product of the electric field $\mathbf{E}$ near the top of chains and the charge ρ of the top bead. The electric field and the induced charge were determined by the following two coupled equations, the Gauss low and the conservation of charge.

$$\nabla \cdot \left(\varepsilon_0 \varepsilon_r \nabla \phi \right) = -\rho, \;\; \nabla \cdot \left(\sigma \nabla \phi \right) = -\frac{\partial \rho}{\partial t}, \qquad (5)$$

where ϕ is potential, ε_0, ε_r, σ and ρ is permittivity in free space, relative dielectric constant, conductivity, and space charge, respectively. The relative dielectric constant was 3.0 for photoreceptor and 10.0 for carrier beads. The conductivity of the beads was 6.61×10^{-8} S/m. An iterative FEM was used to calculate the coupled differential equations.[6] The calculation area was divided into small elements in order to sham spherical beads by quadrilateral or hexahedron elements. The size of the elements was set to be 5–21 μm.

Results and Discussion

Solenoid Coil System

Measured critical electric fields in the solenoid system are plotted in Fig. 7. The field was simply estimated by V/d, where V is applied voltage and d is a gap between the top of the chain and the upper electrode. The critical electric field was increased nonlinearly with the increase in the coil current and the bead diameter.

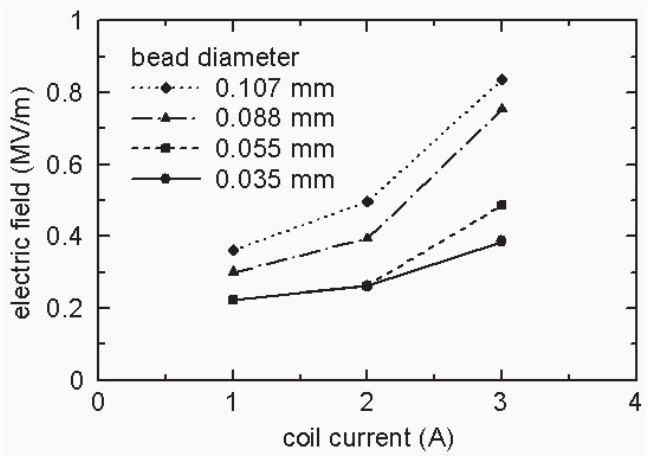

Figure 7. Critical electric field to break chains for various size of bead.

The magnetic and electrostatic forces were calculated on straight parallel chains as shown in Fig. 8. The length of the chains l_c and the interval between chains l_i were adjusted to measured values. The calculation area w was 1 mm. The magnetic force applied to bead "A" at the top of the chain in the center of the area was calculated by Eq. (2). On the other hand, the electrostatic force was deduced by the three-dimensional electric field calculation around chains with measured critical voltage. These two kinds of forces were supposed to balance at the moment when the top bead was separated from the chain.

Figure 9 shows the comparison of calculated magnetic force and electrostatic force. In the figure, a straight line indicates the relation that the calculated magnetic force is equal to the critical electrostatic force. It is clearly recognized from the figure that the result shows a good correlation between the critical electrostatic force and the magnetic bonding force, that is, the calculated curves are almost parallel to the straight line. The result supports the validity of the BCO mechanism shown in Fig. 6. However, the quantitative agreement between magnetic and electrostatic forces is not sufficient and the magnetic forces are overestimated. There are some possible reasons. One is due to modeling error such as the single chain model for actual corn-shaped chains and the approximation by hexahedron elements in the FEM calculation for the sphere beads. In the case of 88 μm beads, for example, the magnetic force calculated by the single chain model is 68% larger than that calculated for corn-shaped chains.[2] The other reason is that since the actual bonding force is determined by many factors such as the chain configuration, physical properties of beads, and shape of beads, which were not identical in the experiment, the most weakly connected bead in numerous beads was pulled-off in the experiment as we observed that a chain is not always broken at the top of the chain but is sometimes broken at the most weakest point in it. On the other hand, because the calculation was conducted under the ideal condition, such as uniform spherical beads in the single-raw chains, the calculated bonding force is larger than the measured weakest one. In any case, we can evaluate the required magnetic field to prevent the BCO by introducing a "safety factor" as we design mechanical structures using brittle materials.

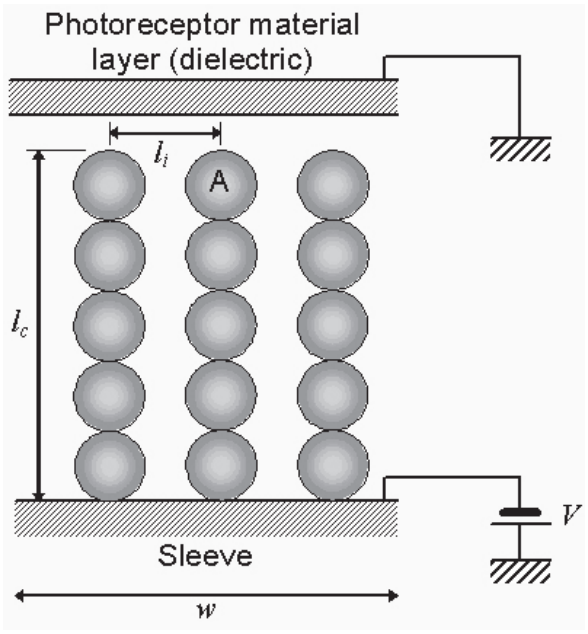

Figure 8. Single chain model for applied force calculation.

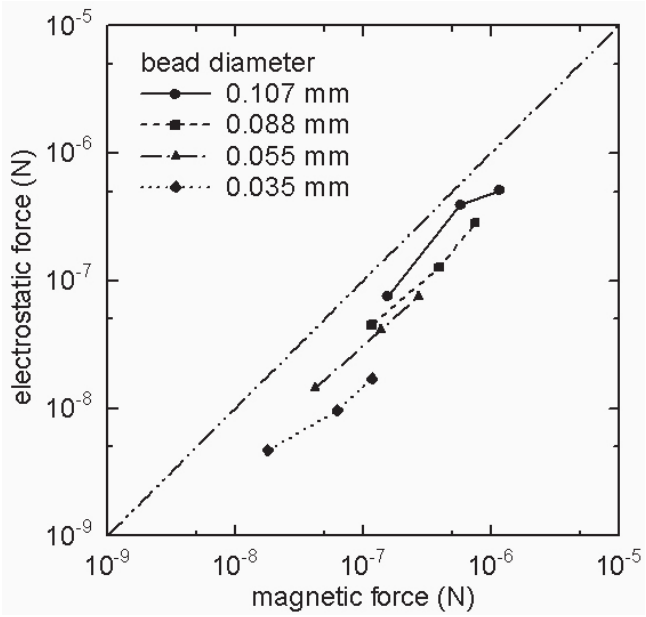

Figure 9. Comparison of electrostatic and magnetic forces for various size of bead.

Magnet Roller System

Figure 10 shows how the weight of electrically pulled-off carrier beads was increased by the applied voltage between the magnet roller and the plate. It is recognized that the critical voltage required to separate chains and the weight of pulled-off carriers was increased with the increase in the applied voltage and the decrease of the bead diameter, i.e., the critical electrostatic pull-off force increased with the increase in the magnetic flux density and the bead diameter. This feature agreed qualitatively with the results obtained in the solenoid coil experiment.

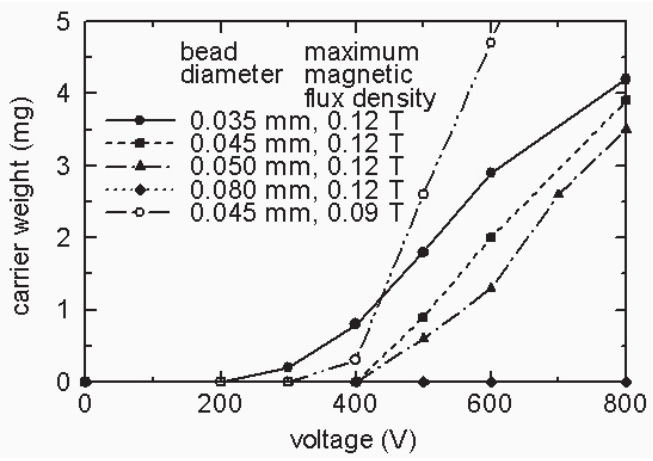

Figure 10. Weight of electrically pulled-off carrier beads. The values indicated in the figure are bead diameters and maximum magnetic flux densities.

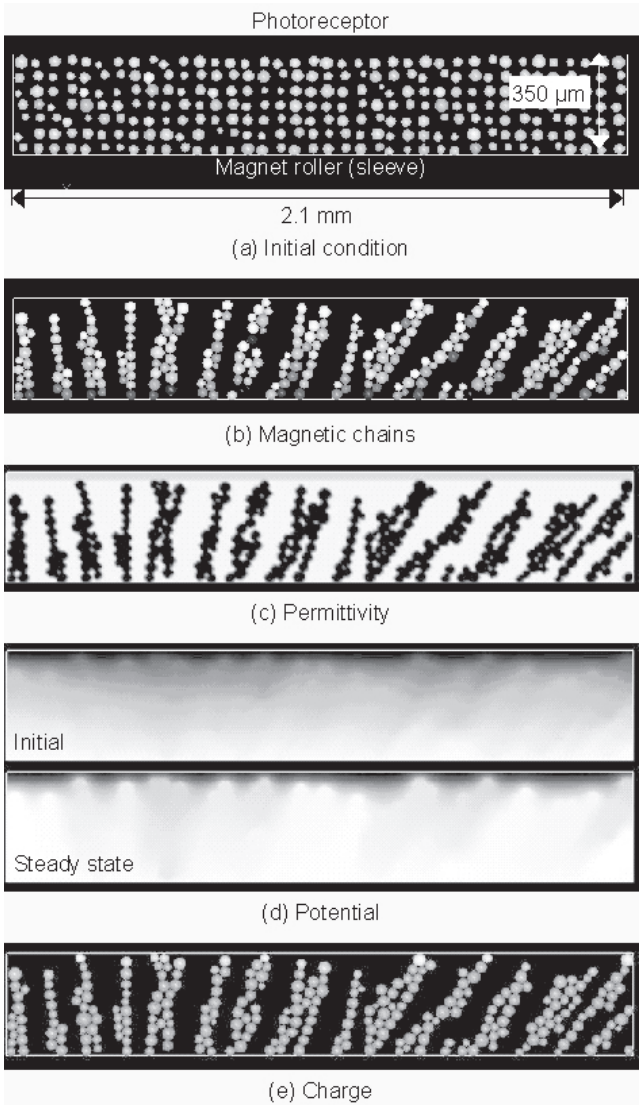

Figure 11. Numerical results of chain forming process and electric field calculation. The averaged bead diameter is 35 μm, standard deviation of diameter is 10%, bead number is 266, and magnetic field is specified by the parameters listed in Table I.

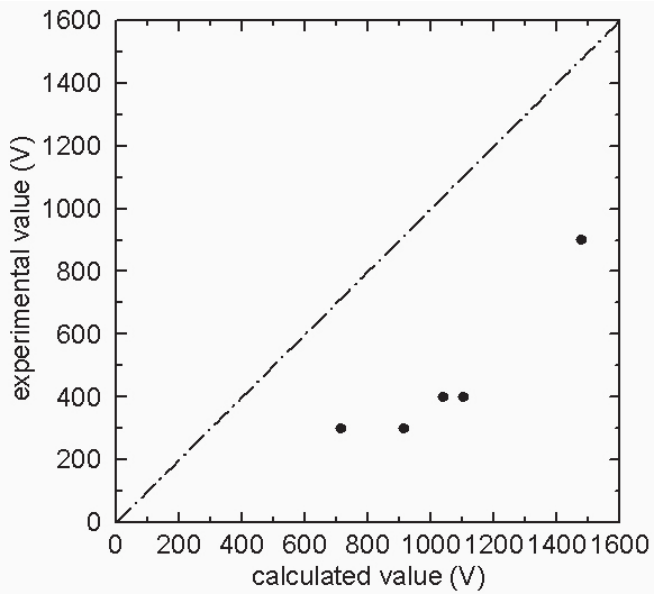

Figure 12. Correlation of calculated and experimental critical pull-off voltage.

Two-dimensional DEM and FEM calculations were performed to compare the results with experimental results in the magnet roller system. At first, chain profiles were determined by the calculation of chain forming process with the DEM. Then induced charge and electrostatic force applied to the beads were determined by electric field calculations with the FEM. Figure 11 shows an example of numerical result. Figure 11(a) is an initial condition of the DEM calculation. The surface of the sleeve was modeled as a flat plate and the center of the figure corresponds to the closest line between magnet roller and plate shown in Fig. 5. Figure 11(b) shows calculated quasi-steady chain profiles at 1 ms after applying magnetic field. In Fig. 11(b), gray level of each carrier bead indicates the magnitude of y-component of magnetic force. At the top of chains where beads are indicated by lower gray level, magnetic force was applied to the beads toward the magnetic roller. Figures 11(c)–11(e) show calculated results on the electrostatic field. Figure 11(c) is permittivity distribution for the calculation and Fig. 11(d) shows potential distributions in the initial condition and the steady state. In the steady condition, potential is uniform inside of bulk chain. As a result, carrier beads charged negatively at the top of each chain as illustrated in Fig. 11(e), where gray level of each bead indicate amount of the charge.

From these numerical calculations, critical pull-off voltages were estimated and then these values were compared to experimental results to confirm the validity of the method. Figure 12 shows the result. Although quantitative agreement is not satisfactory, it shows acceptable correlation between the calculated and measured values, that is, a curve fit of the results gives a line with slope 1 and –601 V intercept. As in the solenoid coil experiment, the magnetic forces were overestimated and the same reasons for discrepancy are expected here. In this case, the intercept is mainly due to a two-dimensional modeling error. Because the existence of beads and the magnetic interaction between beads in perpendicular to the calculation plane are not

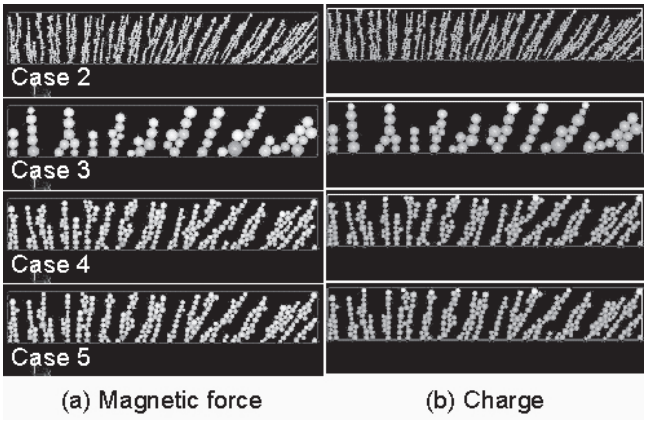

Figure 13. Calculated chain profile and distribution of magnetic force and charge of bead.

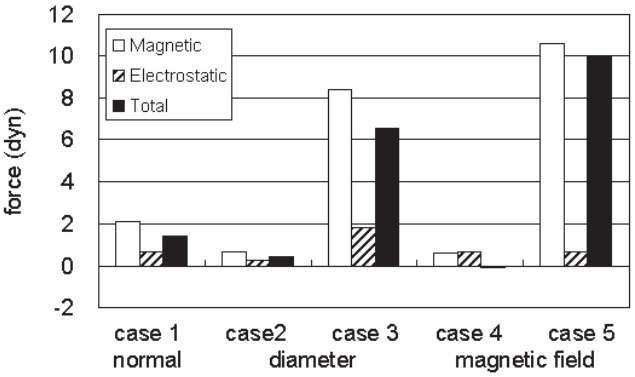

Figure 14. Comparison of calculated magnetic, electrostatic and total forces.

estimated in the two-dimensional calculation, lengths of chains are underestimated as cited in Ref. 2. As a result, the calculated magnetic forces were larger than those obtained with the three-dimensional field. In addition, for this kind of experiment, van der Waals force between photoreceptor material on the flat plate and the beads should be considered in a future study because the beads were attached to soft photoreceptor material and the contact area was increased when the plate was pressed to the bead layer on the sleeve.

The effects of carrier diameter and magnetic field on the applied forces were also investigated by the same procedure mentioned above. The calculated results are shown in Fig. 13. In the figure, magnetic force distribution (Fig. 13(a)) and charge distribution (Fig. 13(b)) are indicated by gray level for each bead. In case 2 and 4, the diameter and the magnetic field were assumed to be one-half of the nominal values. On the other hand, in case 3 and 5, these were assumed to be two times larger than the nominal values. The estimated forces in each case are plotted in Fig. 14. The magnetic forces and total forces are plotted positive toward the magnet roller, while electrostatic forces are plotted positive toward opposite direction. Same as the results in the experiment with the solenoid coil, the diameter and the magnetic field affected pull-off characteristics. The results predict that the large bead and the high magnetic field decrease the amount of pulled-off carriers.

Conclusion

In this study, electrostatic pull-off phenomenon known as bead-carry-out in the two component development process of electrophotography was investigated by two separate experiments and the numerical calculation. From the electrostatic pull-off measurement, it was clarified how the critical pull-off field intensity to break chains and the amount of pulled-off carriers depended on the bead diameter and the magnetic field. Magnetic bonding force and electric pull-off force were estimated numerically to evaluate these experimental results. It was clarified that the bead-carry-out phenomenon cuold be predicted qualitatively from the comparison of calculated magnetic and electrostatic force.

References

1. E. M. Williams, The Physics and Technology of Xerographic Processes, (Krieger Publishing, Maclabar, FL, 1993).
2. N. Nakayama, H. Kawamoto and M. Yamaguchi, "Statics of Magnetic Bead Chain in Magnetic Field", *J. Imaging Sci. Technol.* **46**, 5 , 422-428 (2002).
3. N. Nakayama, H. Kawamoto and S. Yamada, "Resonance Frequency and Stiffness of Magnetic Bead Chain in Magnetic Field", *J. Imaging Sci. Technol.* **47**, 5, 408-417 (2003).
4. P. A. Cundall and O. D. L. Strack, "A Discrete Numerical Model for Granular Assemblies", *Géotechnique* **29**, 1, 47-65 (1979).
5. R. S. Paranjpe and H. G. Elrod, "Stability of Chains of Permeable Spherical Beads in an Applied Magnetic Field", *J. Appl. Phys.* **60**, 1, 418-422 (1986).
6. H. Kawamoto, "Statics of Pin Corona Charger in Electrophotography", *J. Imaging Sci. Technol.* **45**, 6, 556-564 (2001).